JBC RESEARCH ARTICLE

GPR39-mediated molecular signaling by bile acids

Received for publication, May 29, 2025, and in revised form, January 22, 2026 Published, Papers in Press, February 4, 2026
https://doi.org/10.1016/j.jbc.2026.111241

Yanyun Huang[1,2], **Zhentao Zi**[3,4], **Chenliang Xia**[3,4], **and Yi Rao**[1,2,3,4,*]

From the [1]*Department of Pharmacology School of Basic Medical Sciences and Center for AI Therapeutics, Fudan University Shanghai Medical College, Shanghai, China;* [2]*School of Basic Medical Sciences, Chinese Institutes for Medical Research (CIMR), Capital Medical University, Beijing, China;* [3]*Laboratory of Neurochemical Biology, Peking-Tsinghua Center for Life Sciences, PKU-IDG/McGovern Institute for Brain Research, Peking-Tsinghua-NIBS (PTN) Graduate Program, School of Life Sciences, Beijing, China; and* [4]*Department of Chemical Biology, College of Chemistry and Chemical Engineering; School of Pharmaceutical Sciences, Peking University, Beijing, China*

Reviewed by members of the JBC Editorial Board. Edited by Kirill Martemyanov

Bile acids (BAs), long known for roles in food emulsion, also function as biological signals. By measuring intracellular calcium, we have recently discovered that GPR39, a G protein-coupled receptor, is a receptor for 3-O-sulfated BAs including lithocholic acid 3-sulfate (LCAS), taurolithocholic acid 3-sulfate (TLCAS) and glycolithocholic acid 3-sulfate (GLCAS) in cultured cells and in pancreatic acinar cells. We have now used multiple assays from electrophysiologic recording in *Xenopus* oocytes, Ca^{2+} imaging, NanoBiT, ONE-GO, and TANGO to validate GPR39 activation by BAs. Among 30 BAs, only sulfated forms (LCAS, TLCAS and GLCAS) evoked GPR39 activation, activating 9 distinct Gα protein subtypes across the $G\alpha_q$, $G\alpha_i$, and $G\alpha_{12/13}$ subfamilies. LCAS induced phosphorylation of ERK1/2 in the pancreas and the liver, which was markedly attenuated in *Gpr39* knockout mice. Mutagenesis analysis identified the key residues essential for GPR39 signaling. Our results have revealed new signaling molecules downstream of GPR39 activation.

G protein-coupled receptors (GPCRs) play important physiological roles and are the major family of drug targets (1), accounting for ∼36% of all approved therapeutic agents (2). GPR39 was initially identified as a growth hormone secretagogue receptor (GHSR) homolog in the fetal brain (3) and belongs to the class A GPCRs (4). It is expressed in the pancreas, the liver, adipose tissues, the gastrointestinal tract, and the central nervous system (CNS) (5, 6). GPR39 has been reported to be involved in the regulation of cell proliferation, differentiation, survival, apoptosis, ion transport and pH homeostasis (7–12).

Twenty years ago, GPR39 was found to be a receptor for zinc ions (Zn^{2+}) (13, 14). However, the endogenous ligand of GPR39 has been a subject of ongoing debate (15). In 2024, we identified bile acids (BAs) as endogenous ligands for GPR39, with GPR39 from evolutionarily earlier species responding only to BAs but GPR39 from evolutionarily later species responding to both BAs and Zn^{2+} (16). Our previous work showed that BAs, particularly lithocholic acid 3-sulfate (LCAS), glycolithocholic acid 3-sulfate (GLCAS) and taurolithocholic acid 3-sulfate (TLCAS), activated intracellular Ca^{2+} signaling through GPR39 *via* the $G\alpha_q$ pathway, and that GPR39 is necessary and sufficient for BA-induced Ca^{2+} responses in HEK293T cells and pancreatic acinar cells (16). However, Ca^{2+} signaling represents only one facet of GPCR function, and the broader downstream signaling repertoire of GPR39 activation by BAs remains poorly defined. Here, we confirm and extend GPR39 activation by BAs using multiple assays, including the classic *Xenopus* oocytes system, NanoBiT-based Gα and β-arrestin recruitment assays (17), the ONE-GO biosensor for detecting Gα activation (18), and measurements of ERK phosphorylation in primary pancreatic acinar cells and hepatocytes. We have also investigated amino acid residues in the GPR39 protein required for its activation.

Results

BA activation of GPR39 in Xenopus *oocytes demonstrated by electrophysiological recordings*

We have now used the two-electrode voltage-clamp (TEVC) technique with *Xenopus* oocytes, a well-established method for investigating GPCRs activation (19). This technique enabled the detection of ion currents through endogenous calcium-activated chloride channels (CaCCs) (20), activated by $G\alpha_q$-mediated calcium release from the endoplasmic reticulum (Fig. 1*A*). *Xenopus* oocytes provides a classic model to study membrane receptors, with a well-controlled and simplified environment facilitating specific assessment of ligand-receptor activities (21).

To validate GPR39 activation by Zn^{2+}, we injected either mRNA encoding green fluorescent protein (GFP) (Fig. 1*B*) or that encoding GPR39 (Fig. 1*C*) into oocytes. Perfusion of Zn^{2+} induced inward currents exclusively in GPR39-expressing oocytes (Fig. 1*C*), with the half-maximal concentration (EC_{50}) of 114.8 μM (Fig. 1*D*). No response was observed in the GFP-expressing oocytes even at Zn^{2+} concentrations up to 500 μM (Fig. 1*B*). Both the $G\alpha_q$ inhibitor YM254890 (Fig. 1, *B* and *D*) (22) and the CaCCs inhibitor Caccinh-A01 (Fig. 1, *B* and *D*) (23) blocked these currents. The maximal current amplitude activated by 500 μM Zn^{2+} was 883 ± 38.5 nA,

* For correspondence: Yi Rao, yrao@pku.edu.cn.

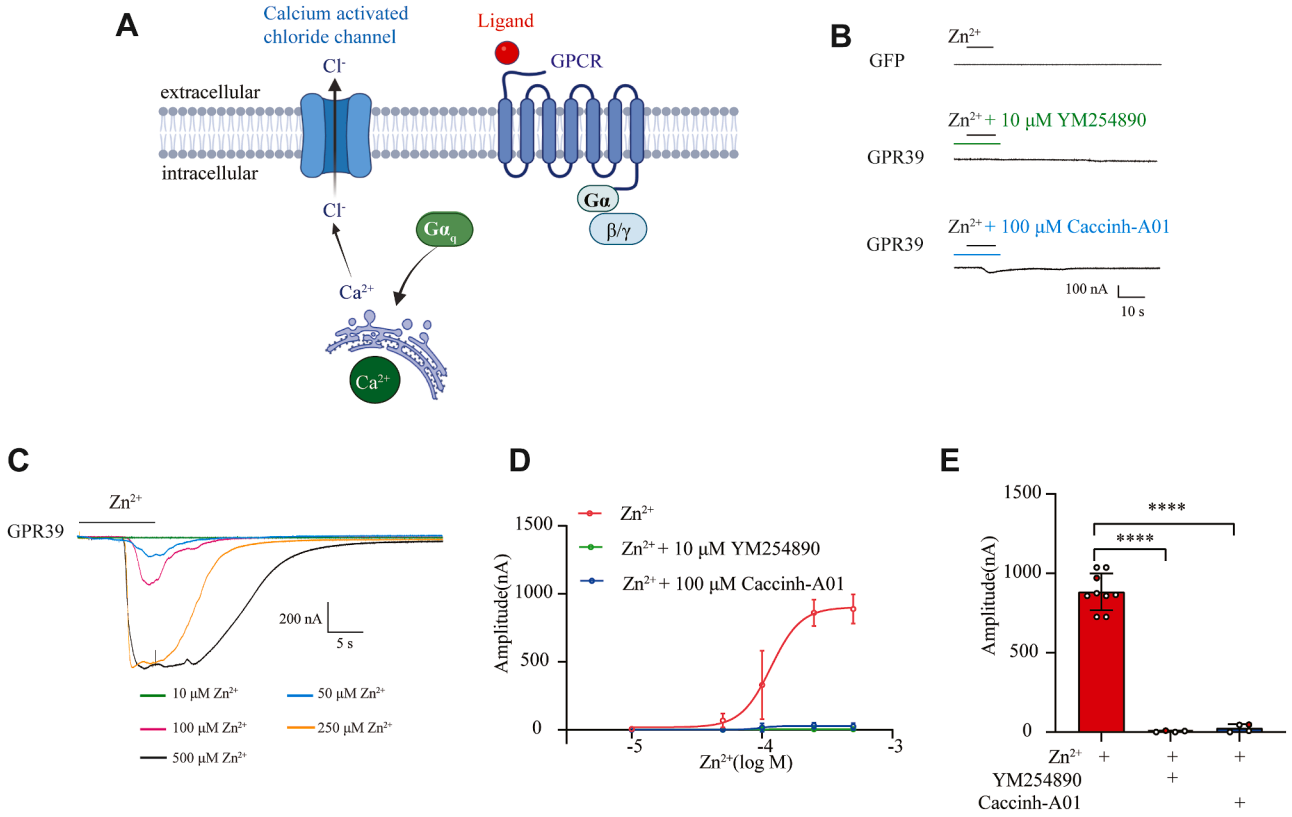

Figure 1. Validation of GPR39 signaling in *Xenopus* oocytes. *A*, a schematic illustration of GPCR-mediated ion channel regulation in the *Xenopus* oocyte system. $G\alpha_q$ type of GPCRs activate of endogenous calcium-activated chloride channels (CaCCs). *B*, representative current traces recorded from oocytes injected with mRNAs encoding the *green* fluorescent protein (GFP) or GPR39, treated with 500 μM Zn^{2+} and pre-incubated with 10 μM $G\alpha_q$ inhibitor YM254890 or 100 μM CaCCs inhibitor Caccinh-A01. *C*, representative current traces recorded from GPR39-expressing oocytes treated with Zn^{2+}. *D*, dose-response curves Zn^{2+}-induced currents in GPR39-expressing oocytes: curves correspond to Zn^{2+} alone, or Zn^{2+} combined with 10 μM YM254890 or 100 μM Caccinh-A01. *E*, statistical analysis of current amplitudes after 500 μM Zn^{2+} treatment in the presence of 10 μM YM254890 or 100 μM Caccinh-A01, data were expressed as mean ± standard deviation (SD) (N ≥ 3). One-way ANOVA test was used, **** indicates $p < 0.0001$. The p values of Zn^{2+} *versus* YM254890 and Caccinh-A01 were both < 0.0001.

which was reduced to 4.65 ± 2.17 nA by 10 μM YM254890 ($p < 0.0001$, Fig. 1*E*) and to 25.3 ± 12.2 nA by 100 μM Caccinh-A01 ($p < 0.0001$, Fig. 1*E*). These pharmacological results suggested that *Xenopus* oocytes provide a reliable system for validating GPR39 activation.

Next, we examined the effect of LCAS on GPR39 activation in oocytes. LCAS elicited dose-dependent inward currents in GPR39-expressing oocytes (Fig. 2*B*) but failed to induce responses in GFP-expressing oocytes even at LCAS concentrations up to 500 μM (Fig. 2*A*). EC_{50} for GPR39 activation by LCAS was 117 μM (Fig. 2*C*). LCAS-induced currents were inhibited by YM254890 (Fig. 2, *A* and *C*) and Caccinh-A01 (Fig. 2, *A* and *C*). The maximal current amplitude induced by 500 μM LCAS was 838 ± 54.7 nA, which was reduced to 18.7 ± 13.7 nA by 10 μM YM254890 ($p < 0.0001$, Fig. 2*D*) and to 25.1 ± 14.5 nA by 100 μM Caccinh-A01 ($p < 0.0001$, Fig. 2*D*). These results provide further evidence that LCAS is a ligand for GPR39.

In addition, exogenous G protein-gated inwardly rectifying potassium channels (GIRKs) can be activated after Gβγ dimers dissociated from $G\alpha_i$ (Fig. 2*E*). To test whether LCAS activation of GPR39 also couples to $G\alpha_i$ signaling pathway, we injected mRNAs for two subunits of GIRK, GIRK1S and GIRK3, along with that for GPR39 into oocytes. Perfusion of 250 μM LCAS in high potassium media elicited a distinct current (Fig. 2*F*), which was blocked by pertussis toxin (PTX), a common inhibitor of $G\alpha_i$. The maximal current amplitude induced by 250 μM LCAS was 491.3 ± 42.8 nA, which was reduced to 237.6 ± 30.7 nA by 100 ng/ml PTX ($p < 0.001$, Fig. 2*G*). Taken together, these results indicate that $G\alpha_q$ and $G\alpha_i$ subunits are downstream of LCAS activated GPR39 signaling.

GPR39 recruitment of $G\alpha_q$, $G\alpha_i$, and $G\alpha_{12/13}$ proteins after LCAS activation

Biased signaling of GPCRs is known with different agonists activating different signaling pathways downstream of the same GPCR (24, 25), including differential recruitments of Gα proteins and β-arrestins (26, 27). Heterotrimeric G proteins are composed of α, β and γ subunits; both Gα-GTP and Gβγ dimers are both capable of regulating downstream effector functions (28). Among them, Gα proteins can be divided into $G\alpha_{q/11}$ family, $G\alpha_{i/o}$ family, $G\alpha_s$ family and $G\alpha_{12/13}$ family. The human genome encodes 16 isoforms of Gα proteins, 5 isoforms of Gβ proteins and 12 isoforms of Gγ proteins (29).

To systematically investigate downstream signaling pathways activated by GPR39, we first utilized the NanoBiT assay to monitor the recruitment of four major Gα families

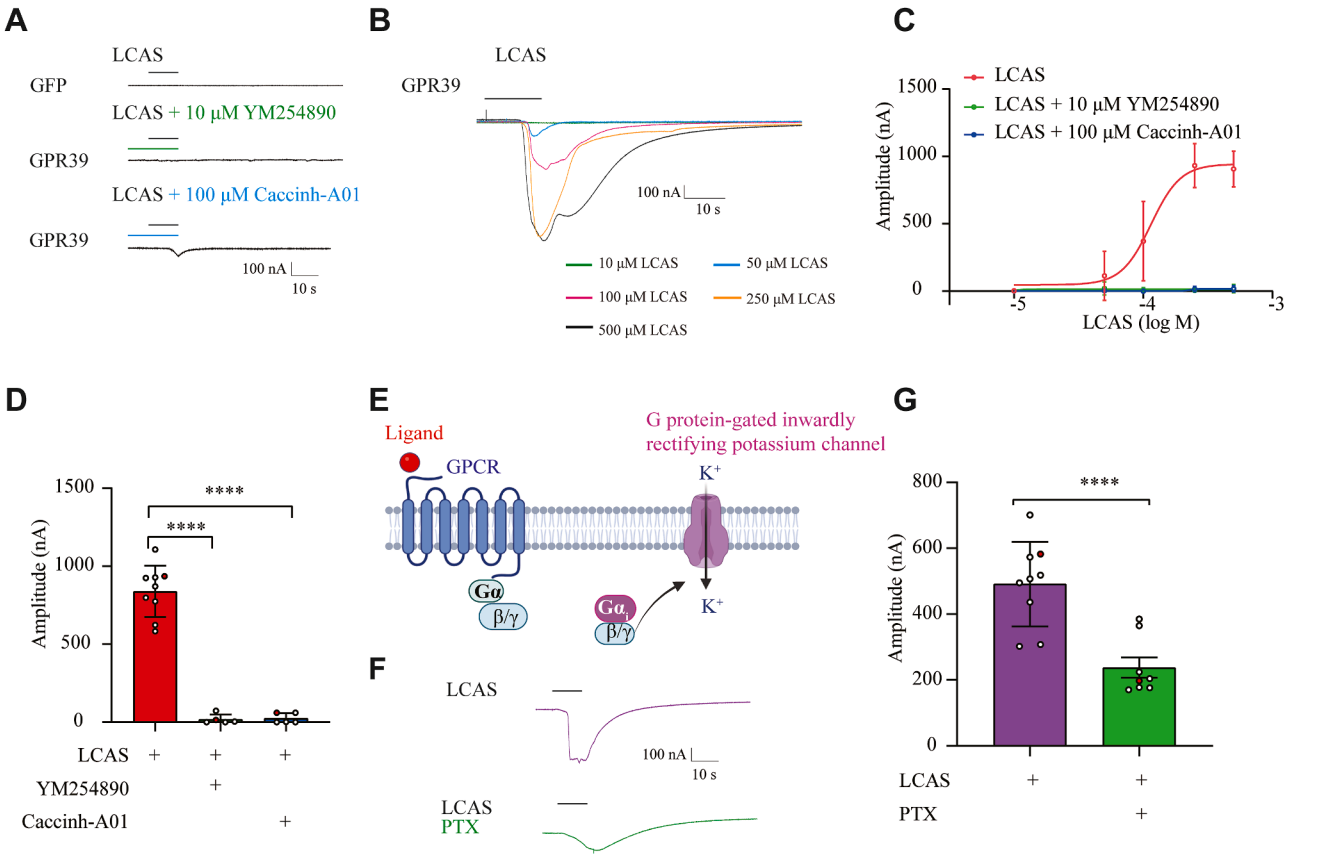

Figure 2. LCAS as a ligand for GPR39 expressed in *Xenopus* oocytes. *A*, representative current traces recorded from oocytes injected with mRNAs encoding the GFP or GPR39: traces correspond to 500 μM LCAS treatment, with/without pre-incubation of 10 μM $G\alpha_q$ inhibitor YM254890 or 100 μM CaCCs inhibitor Caccinh-A01. *B*, representative current traces recorded from GPR39-expressing oocytes, stimulated with various concentrations of LCAS (10 μM, 50 μM, 100 μM, 250 μM, 500 μM). *C*, dose-response curves of LCAS-induced current amplitudes in GPR39-expressing *Xenopus* oocytes: curves reflect LCAS alone, or LCAS combined with 10 μM YM254890 or 100 μM Caccinh-A01. *D*, statistics analysis of current amplitudes in GPR39-expressing *Xenopus* oocytes treated with 500 μM LCAS (with/without 10 μM YM254890 or 100 μM Caccinh-A01), data were expressed as mean ± SD (N ≥ 3). One-way ANOVA test was used, **** indicates $p < 0.0001$. The *p* values of LCAS *versus* YM254890 and Caccinh-A01 were all < 0.0001. *E*, a schematic illustration of *Xenoupus* oocyte expression of exogenous G protein-gated inwardly rectifying potassium (GIRK) channels. *F*, representative current traces recorded from oocytes co-expressing GIRK1S, GIRK3 and GPR39, stimulated with LCAS, with/without overnight pretreatment with 100 ng/ml PTX. *G*, statistical analysis of current amplitudes in oocytes co-expressing GIRK1S, GIRK3 and GPR39: groups correspond to LCAS stimulation (with/without 100 ng/ml PTX pretreatment). Data are expressed as mean ± SD (N ≥ 3). Statistical comparisons were performed using a two-tailed *t* test (*** indicates $p <$ 0.001). The exact *p*-value for the LCAS *versus* PTX group was 0.0003.

($G\alpha_q$, $G\alpha_i$, $G\alpha_s$, and $G\alpha_{12}$) upon LCAS activation (17). Upon LCAS stimulation, GPR39 recruited $G\alpha_q$, $G\alpha_i$, and $G\alpha_{12}$ proteins but not $G\alpha_s$ (Figs. 3*A* and S1). While $G\alpha_q$ showed the highest maximal response (E_{max} = 1.58 Fig. 3*C*), $G\alpha_i$ displayed the highest potency with an EC_{50} of 58.0 ± 10.6 μM, followed by $G\alpha_q$ (70.2 ± 10.4 μM) and $G\alpha_{12}$ (73.0 ± 17.2 μM) (Fig. 3*D*). A radar plot analysis based on the log (RA_i) (30) confirmed that GPR39 couples strongly to $G\alpha_i$ and $G\alpha_q$ (Fig. 3*B*).

To further refine our understanding of Gα protein signaling of GPR39, we used the ONE-GO biosensors (Fig. 3*E*), which can detect the activation of 10 Gα isoforms (18) (Fig. 3*F*). We found that LCAS-activated GPR39 engaged a broad spectrum of Gα proteins, including $G\alpha_q$, $G\alpha_{i/o}$ family ($G\alpha_{i1}$, $G\alpha_{i2}$, $G\alpha_{i3}$, $G\alpha_{oA}$, $G\alpha_{oB}$, $G\alpha_z$) and $G\alpha_{12/13}$ family ($G\alpha_{12}$ and $G\alpha_{13}$) (Fig. 3*G*).

In addition to G protein pathways, β-arrestin signaling represents another major downstream pathway following GPCR activation (31, 32). To detect β-arrestin-1 and -2 recruitment, we used the NanoBiT method (33). We observed that LCAS induced weak recruitment of both β-arrestin-1 and -2, with the EC_{50} values of 125 μM and 40.5 μM, respectively (Fig. S2, *A* and *B*). Zn^{2+} alone did not induce β-arrestin-1 or -2 recruitment to GPR39, however, co-application of 4 μM Zn^{2+} significantly enhanced LCAS-induced β-arrestin-1 and -2 recruitment (Fig. S2, *A* and *B*).

Comparison of BAs in activating signaling downstream of GPR39

BAs are produced from cholesterol in the liver (34), stored in the gallbladder, and enter intestine (35), where they are modified by intestinal bacteria to produce secondary BAs (36). To systematically investigate the effects of BAs on downstream signaling mediated by GPR39, we screened the recruitment of Gα proteins induced by 30 different BAs using NanoBiT assay (Fig. 4*A*). Recruitment of $G\alpha_q$, $G\alpha_i$ and $G\alpha_{12}$ to GPR39 was observed upon stimulation with the three sulfated BAs (LCAS, TLCAS, and GLCAS) (Fig. 4*A*). No significant differences were observed among these three sulfated BAs in recruiting $G\alpha_q$ (Fig. 4*B*). For $G\alpha_i$, LCAS exhibited the highest potency (Fig. 4*C*). $G\alpha_{12}$ was weakly recruited by

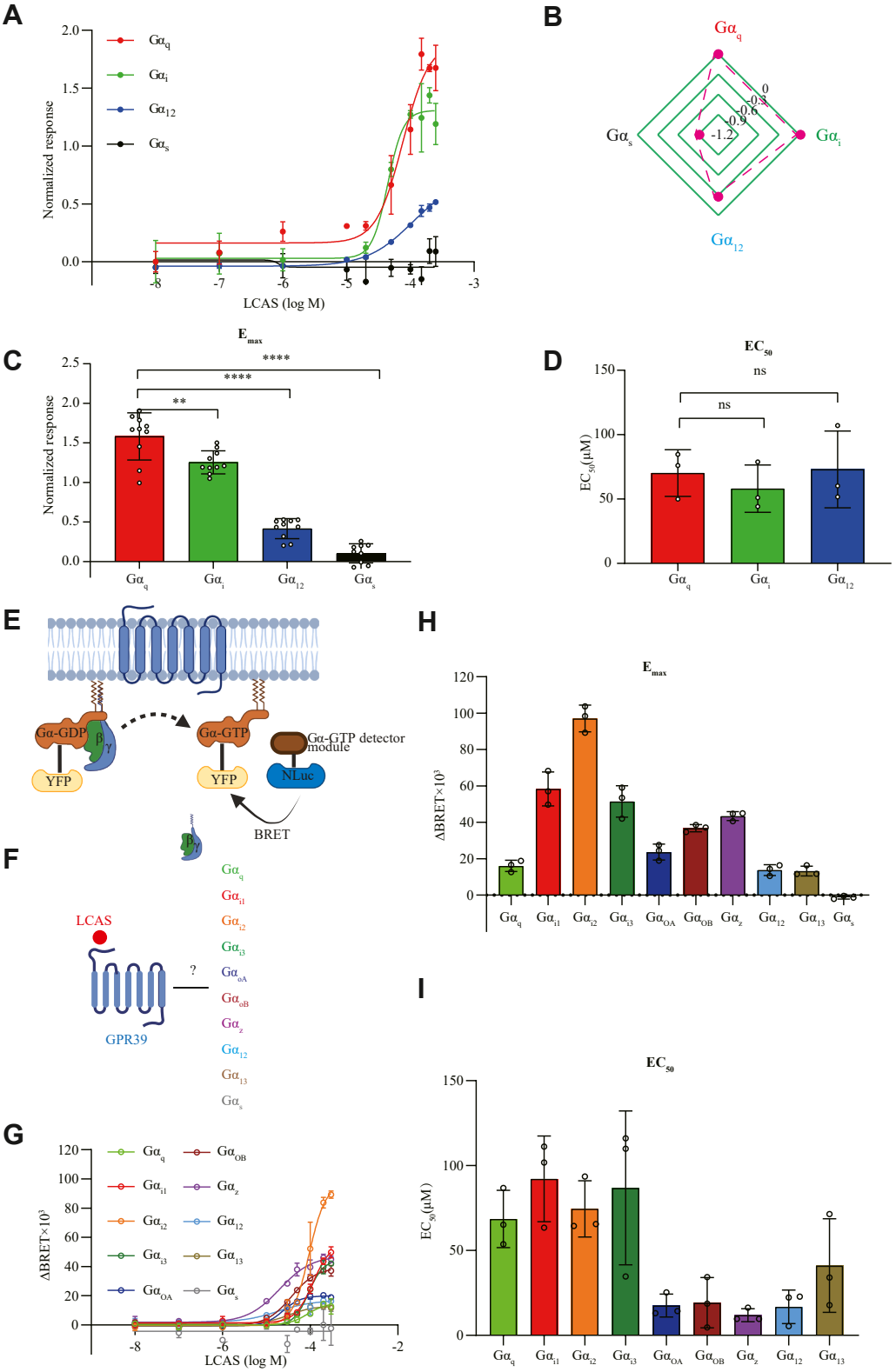

Figure 3. Recruitment of $G\alpha_q$, $G\alpha_i$, and $G\alpha_{12/13}$ by GPR39 after LCAS activation. *A*, dose-responses for GPR39 activation by LCAS, as detected by the NanoBiT assay, showing recruitment of Gα proteins. Data were normalized to the HBSS group. *B*, a radar plot showing recruitment efficiencies of different Gα proteins by LCAS-activated GPR39. Recruitment strength for each Gα protein was expressed as the log of the response efficacy (log[RAi]). *C*, E_{max} of GPR39 activation by LCAS for different Gα proteins, based on the NanoBiT assay. Data from 3 independent replicate experiments with 3 replicate wells at the 250 μM, N = 9, mean ± SD. Data were normalized to the HBSS group. One-way ANOVA test was used, ** indicates $p < 0.01$, **** indicates $p < 0.0001$. The *p* values of $G\alpha_i$, $G\alpha_{12}$ and $G\alpha_s$ *versus* $G\alpha_q$ were 0.0013, < 0.0001 and < 0.0001. *D*, EC_{50} of GPR39 activation by LCAS for different Gα proteins, based on the NanoBiT assay. N = 3, mean ± SD. One-way ANOVA test was used, ns indicates $p > 0.05$. The *p* values of $G\alpha_i$ and $G\alpha_{12}$ *versus* $G\alpha_q$ were 0.7487 and 0.9834. *E*, a schematic diagram of the ONE-GO assay, illustrating energy resonance transfer between the nanoluc (Nluc) and yellow fluorescent protein (YFP) peptides for detecting Gα protein recruitment after GPCR activation. *F*, classification of Gα proteins activated by LCAS *via* GPR39, as determined by

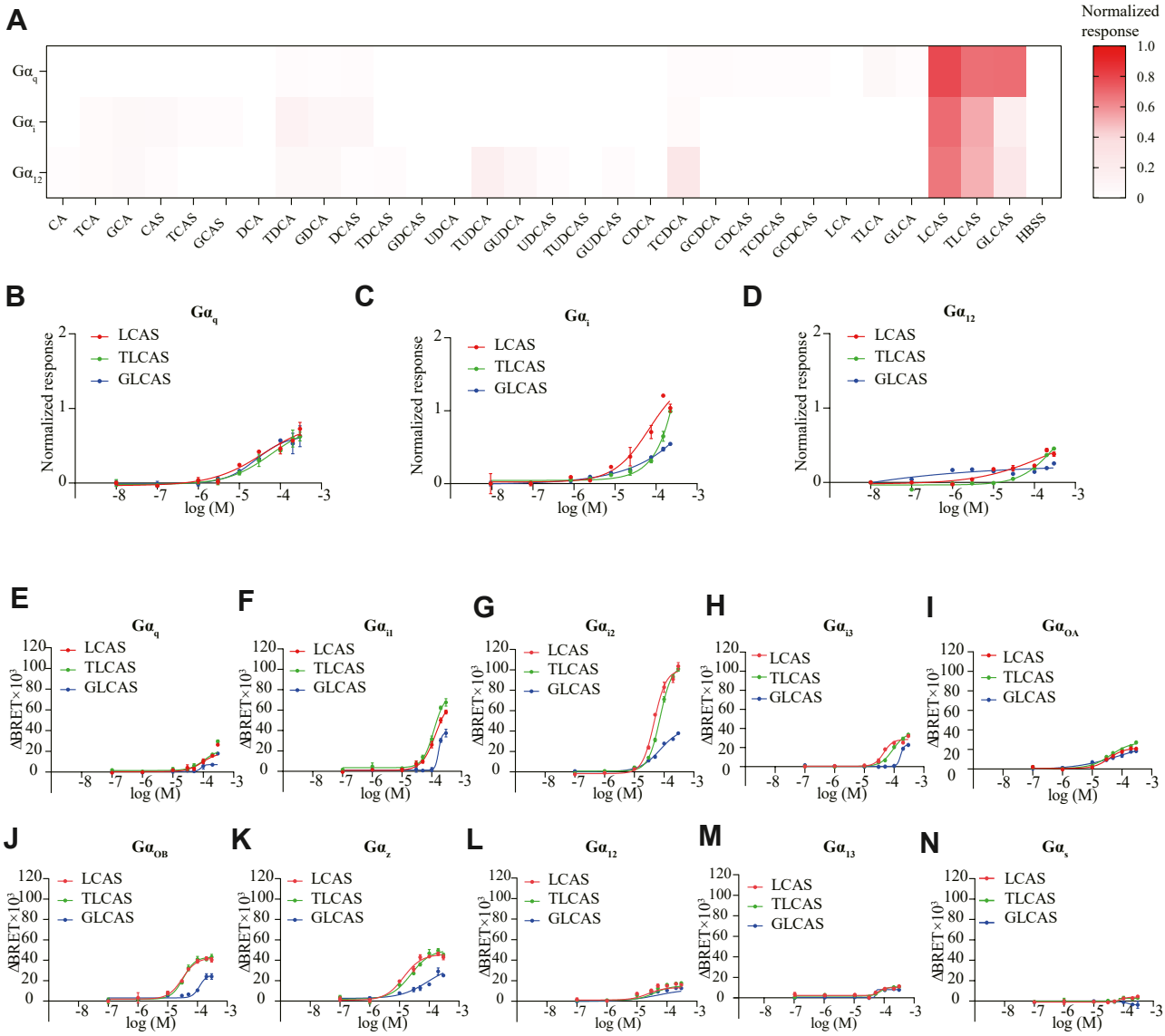

Figure 4. Gα protein recruitment after BAs activation of GPR39. *A*, a heatmap of Gα proteins recruitment by GPR39 after activation by BAs based on NanoBiT assay. Each BA was tested at 200 μM in triplicate. Data were normalized to the HBSS group. *B–D*, dose-response curves showing the activation of GPR39 and recruitment of $G\alpha_q$ (*B*), $G\alpha_i$ (*C*), and $G\alpha_{12}$ (*D*) proteins based on NanoBiT assay by LCAS, TLCAS and GLCAS. N = 3, mean ± SD. Data were normalized to the HBSS group. *E–N*, BRET in HEK293T cells expressing GPR39 along with ONE-GO biosensors $G\alpha_q$ (*E*), $G\alpha_{i1}$ (*F*), $G\alpha_{i2}$ (*G*), $G\alpha_{i3}$ (*H*), $G\alpha_{oA}$ (*I*), $G\alpha_{oB}$ (*J*), $G\alpha_z$ (*K*), $G\alpha_{12}$ (*L*), $G\alpha_{13}$ (*M*), and $G\alpha_s$ (*N*) upon stimulation with LCAS, TLCAS and GLCAS. Each concentration was measured in triplicate. N = 3, mean ± SD.

GPR39 after stimulation with any of these sulfated BAs (Fig. 4*D*).

We further examined Gα protein activation by the three BAs using the ONE-GO assay. LCAS, TLCAS, and GLCAS activated $G\alpha_q$, $G\alpha_{i/o}$ ($G\alpha_{i1}$, $G\alpha_{i2}$, $G\alpha_{i3}$, $G\alpha_{oA}$, $G\alpha_{oB}$, $G\alpha_z$), and $G\alpha_{12/13}$ ($G\alpha_{12}$ and $G\alpha_{13}$) family members, but failed to activate $G\alpha_s$ protein. These results were consistent with the NanoBiT-based G protein recruitment assays. Our systematic analysis indicates that among BA-GPR39 signaling, the sulfated BAs LCAS, TLCAS, and GLCAS are potent agonists of GPR39 and preferentially signal through $G\alpha_q$, $G\alpha_i$ and $G\alpha_{12/13}$ pathway.

Differential signaling initiated by LCAS and Zn^{2+} activation of GPR39

To compare G protein coupling preferences between Zn^{2+} and LCAS, Zn^{2+} induced GPR39 signaling was analyzed using the ONE-GO assay. We found that Zn^{2+} activated a broad spectrum of G proteins, including $G\alpha_q$, $G\alpha_{i/o}$ ($G\alpha_{i1}$, $G\alpha_{i2}$,

the ONE-GO assay. *G*, BRET in HEK293T cells expressing GPR39 along with different ONE-GO biosensors upon LCAS stimulation. Each concentration was measured in triplicate. N = 3, mean ± SD. *H*, E_{max} of GPR39 activation by LCAS for different Gα proteins, based on the ONE-GO assay. Data from 3 independent replicate experiments, N = 3, mean ± SD. *I*, EC_{50} of GPR39 activation by LCAS for different Gα proteins, based on the ONE-GO assay. N = 3, mean ± SD.

$G\alpha_{i3}$, $G\alpha_{oA}$, $G\alpha_{oB}$, $G\alpha_z$), and $G\alpha_{12/13}$ ($G\alpha_{12}$, and $G\alpha_{13}$) family members, but not $G\alpha_s$ (Fig. 5, *A–J*). Ranked by maximal responses, the majority of Gα proteins activated after Zn^{2+} treatment of GPR39 were similar to those downstream of LCAS activation of GPR39 (Fig. 5*K*). However, LCAS elicited significantly higher E_{max} values for the 3 $G\alpha_i$ isoforms ($G\alpha_{i1}$, $G\alpha_{i2}$, and $G\alpha_{i3}$) compared to Zn^{2+} (Fig. 5*K*). Notably, Zn^{2+} showed lower EC_{50} values (indicating higher potency) than LCAS across all Gα proteins (Fig. 5*L*). Details of Gα protein activation by GPR39 in response to LCAS and Zn^{2+} are listed in Table S1.

GPR39 residues required for BA and Zn^{2+} signaling

To search for important residues responsible for GPR39 activation, we performed multiple sequence alignments of GPR39 proteins from different species (Fig. 6*A*), and we generated 21 mutants carrying single amino acid residue changes and 2 mutants carrying double residue changes. We quantified their responses to LCAS and Zn^{2+} using Ca^{2+} imaging (Fig. 6, *B*–G). These 25 residues were highly conserved across species (Fig. S3*A*) and located in the orthosteric ligand-binding pocket of the Class A GPCRs (37).

Mutations at these conserved residues attenuated the E_{max} of GPR39 response to LCAS and Zn^{2+}. For both LCAS (upper panel of Fig. 6*H*) and Zn^{2+} (upper panel of Fig. 6*I*), most mutants exhibited lower maximal responses compared to the wild type (WT). To rule out expression defects, we assessed the surface expression of all mutant proteins by ELISA. With the exception of L170A, I224A/F225A, R303A, and F115A/Y334A, which displayed less than 70% of the WT expression level, the remaining mutants showed efficient membrane localization (Fig. S5*D*).

Among these, mutations in residues R302 and E116 caused the most pronounced effects on the E_{max} of GPR39: the E_{max} of R302A and E116A to LCAS were reduced to less than one-third of that of the WT (upper panel of Fig. 6*H*), and both mutants completely lost responses to Zn^{2+} (upper panel of Fig. 6*I*). V166A and Y334A mutants significantly increased EC_{50} values of LCAS (lower panel of Fig. 6*H*), while W217A, F115A and K309A increased EC_{50} values of Zn^{2+} (lower panel of Fig. 6*I*).

As shown in the scatter plots, a strong correlation was observed between the E_{max} of mutants induced by LCAS and that by Zn^{2+} (Fig. 6*K*). However, the changes in EC_{50} of mutants showed a much weaker correlation (Fig. 6*J*).

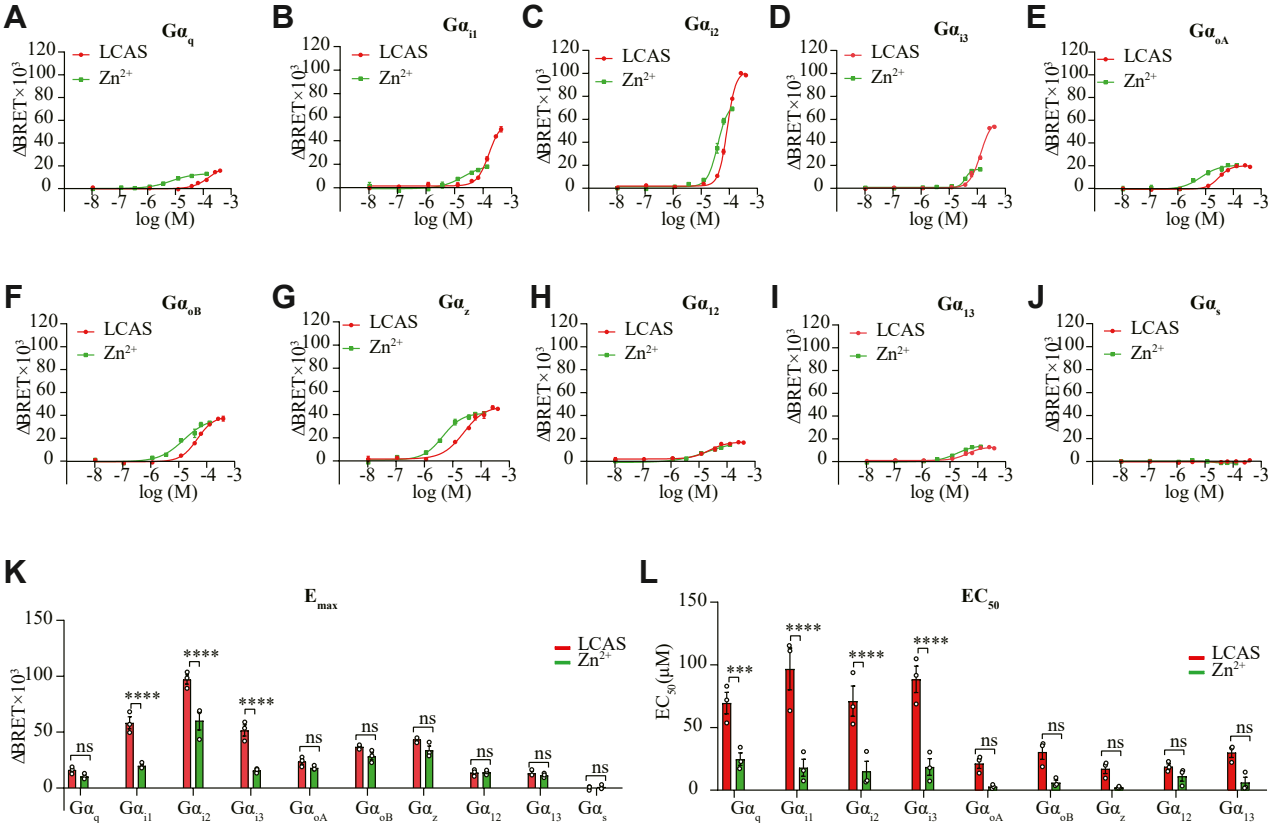

Figure 5. Signaling pathways activated by LCAS and Zn^{2+} *via* GPR39. *A–J*, BRET in HEK293T cells expressing GPR39 along with different ONE-GO biosensors $G\alpha_q$ (*A*), $G\alpha_{i1}$ (*B*), $G\alpha_{i2}$ (*C*), $G\alpha_{i3}$ (*D*), $G\alpha_{oA}$ (*E*), $G\alpha_{oB}$ (*F*), $G\alpha_z$ (*G*), $G\alpha_{12}$ (*H*), $G\alpha_{13}$ (*I*), and $G\alpha_s$ (*J*) upon stimulation with LCAS and Zn^{2+}. Each concentration was measured in triplicate. N = 3, mean ± SD. *K*, E_{max} of GPR39 activation by LCAS and Zn^{2+} for different Gα proteins, based on the ONE-GO assay. N = 3, mean ± SD. Two-way ANOVA with Tukey's multiple comparisons posttest was used, ns indicates $p > 0.05$, * indicates $p < 0.05$, *** indicates $p < 0.001$, **** indicates $p < 0.0001$. The *p* values of $G\alpha_{i1}$, $G\alpha_{i2}$ and $G\alpha_{i3}$ of LCAS *versus* Zn^{2+} were all < 0.0001. The *p* values of $G\alpha_{12}$, $G\alpha_{13}$ and $G\alpha_s$ of LCAS *versus* Zn^{2+} were all > 0.9999. The *p* values of $G\alpha_q$, $G\alpha_{oA}$, $G\alpha_{oB}$ and $G\alpha_z$ of LCAS *versus* Zn^{2+} were 0.8991, 0.9226, 0.4728 and 0.3154. *L*, EC_{50} of GPR39 activation by LCAS and Zn^{2+} for different Gα proteins, based on the ONE-GO assay. N = 3, mean ± SD. Two-way ANOVA with Tukey's multiple comparisons posttest was used, ns indicates $p > 0.05$, ** indicates $p < 0.01$, **** indicates $p < 0.0001$. The *p* values of $G\alpha_{i1}$, $G\alpha_{i2}$ and $G\alpha_{i3}$ of LCAS *versus* Zn^{2+} were all < 0.0001. The *p* values of $G\alpha_q$, $G\alpha_{oA}$, $G\alpha_{oB}$, $G\alpha_z$, $G\alpha_{12}$ and $G\alpha_{13}$ of LCAS *versus* Zn^{2+} were 0.0007, 0.5059, 0.1692, 0.7625, 0.9956 and 0.1881.

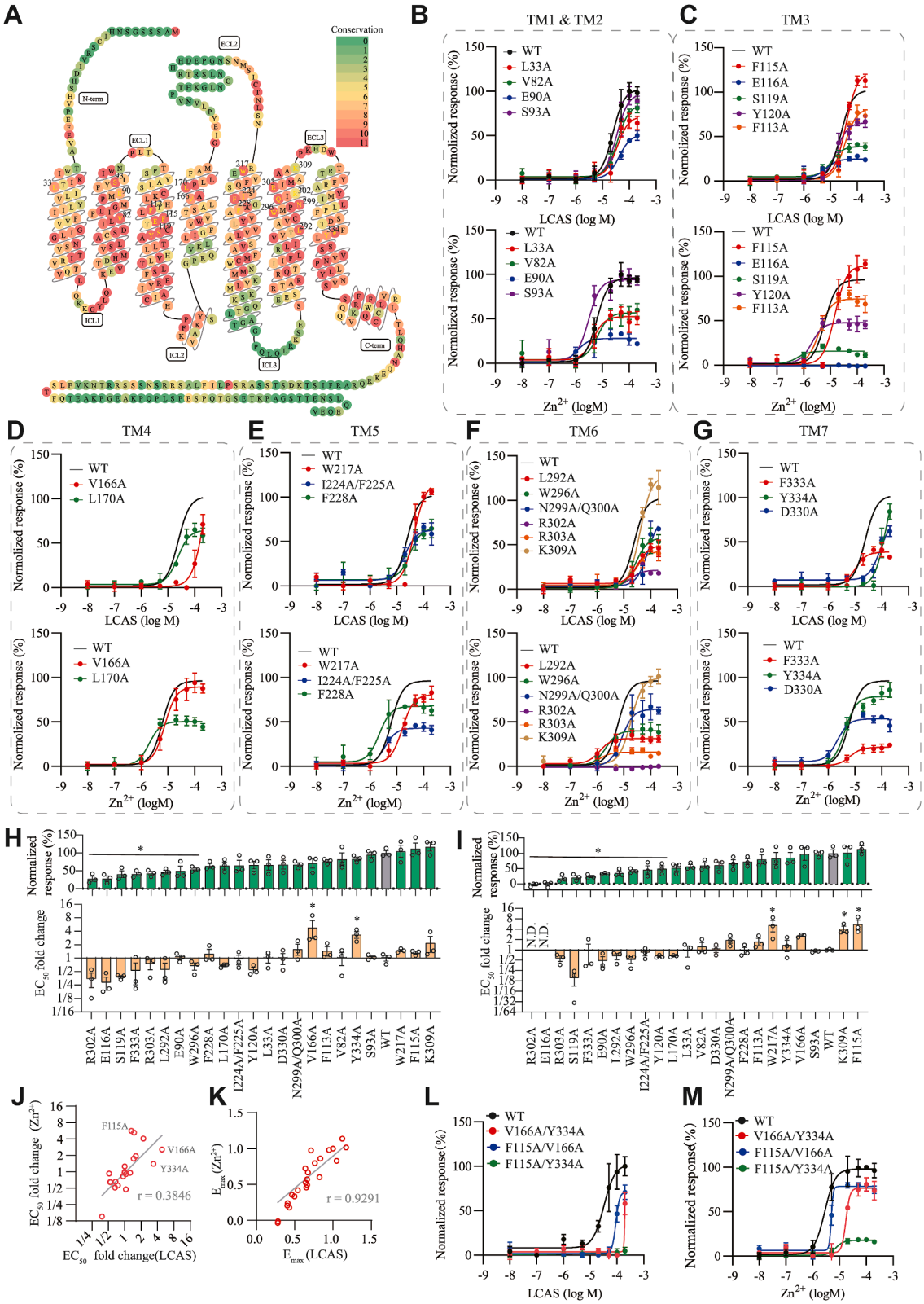

Figure 6. Amino acid residues in GPR39 involved in LCAS and Zn^{2+} activation. *A*, a snake plot of mouse GPR39. Amino acid residues are colored according to their conservation across species. Single letter amino acid codes in *yellow* indicate residues mutated to alanine in this study and the numbers represent residue positions. *B–G*, responses of GPR39 mutants to LCAS and Zn^{2+} activation: (*B*) TM-1/2 mutants (L33A, V82A, E90A, S93A), (*C*) TM-3 mutants (F115A, E116A, S119A, Y120A, F113A), (*D*) TM-4 mutants (V166A, L170A), (*E*) TM-5 mutants (W217A, I224A/F225A, F228A), (*F*) TM-6 mutants (L292A, W296A, N299A/Q300A, R302A, R303A, K309A), (*G*) TM-7 mutants (D330A, F333A, Y334A). Data were normalized to the response of WT GPR39 as 100%. *H* and *I*, efficacy and EC_{50} of responses of GPR39 mutants to LCAS and Zn^{2+}. Efficacy was normalized to the response of WT GPR39 as 100%. N = 3, mean ± SD. One-way ANOVA test was used, * indicates statistical differences, details of *p* value were shown in Table S2. EC_{50} were normalized to WT GPR39. N = 3, mean ± SD. *J*, scatterplots and linear fitting of EC_{50} change fold of Zn^{2+} conditioned to EC_{50} change fold of LCAS among different mutants. *K*, scatterplots and linear fitting of efficacy of Zn^{2+} conditioned to efficacy of LCAS. *L* and *M*, dose-curves of double-point GPR39 mutants (F115A/V166A, V166A/Y334A, F115A/Y334A) induced by LCAS and Zn^{2+}. Data were normalized to the response of WT GPR39 as 100%. N = 3, mean ± SD.

Among these, the F115A, Y334A, and V166A mutants deviated notably from the central line (Fig. 6*J*), indicating that these residues mediated biased responses of GPR39 toward either LCAS or Zn^{2+}. We generated three double-residue mutants by combining these residues in pairs. While individual mutations at these three sites had little effect on the E_{max} of GPR39 (Fig. 6, *H* and *I*), all double mutants exhibited reduced E_{max} compared with the WT (Fig. 6, *L* and *M*). F115A/Y334A mutant nearly lost responsiveness to LCAS rather than Zn^{2+}, likely due in part to decreased membrane expression (Fig. S5*D*). Furthermore, the V166A/Y334A mutant showed diminished sensitivity to LCAS, yet retained partial activation by Zn^{2+}. Details of mutant responses to LCAS and Zn^{2+} were listed in Table S2.

To gain further insight into the mechanism of GPR39 activation, we modeled the structure of GPR39 with AlphaFold 3 server. Because structural predictions for flexible regions were less reliable, the submitted sequence excluded the flexible N- and C-terminal regions. In addition, the longer ECL2 of mouse GPR39 was replaced with the shorter ECL2 from zebrafish GPR39 (Fig. S3*B*). Using AlphaFold3, which allowed ion inclusion in the input sequence, we obtained a GPR39 model with Zn^{2+} coordinates (Fig. S3, *D* and *E*). Then we performed molecular docking of LCAS to the AlphaFold3-derived GPR39 structure using Diffdock-L (38). Among the top five docking poses, four positioned LCAS at the periphery of the receptor, while the Rank2 pose placed LCAS within the receptor at the canonical binding pocket (Fig. S3*E*), which coordinated with our mutagenesis data, and we chose Rank2 pose for further analysis.

AlphaFold3-predicted Zn^{2+} site was adjacent to the DiffDock-predicted LCAS pose, with R302 located within 4 Å of both (Fig. S4, *A* and *B*). Additionally, E90, F115, E116, R303 and D330 were also included in the predicted binding sites (Fig. S4, *C* and *D*). Our previous results showed that mutation at E90, E116 and R303 sites impaired the GPR39 activation by LCAS and Zn^{2+} (Fig. 6, *B*, *C* and *F*). Meanwhile, E90, E116, F115 and D330 sites were also reported to be essential to the activation of GPR39 by a synthetic agonist comp-5 (39).

Based on the modeling and mutagenesis data, we proposed a preliminary activation mechanism for GPR39. In the resting state, R302 and R303 on TM6 interacted with D330 on TM7 and E116 on TM3, respectively, stabilizing the TM6 conformation. Upon binding of Zn^{2+} and LCAS within the pocket, these interactions (R302-D330 and R303-E116) were disrupted, leading to conformational changes and outward displacement of TM6, thereby triggering receptor activation. We refered to this model as the "still-rings" model, as R302 and R303 supported the stability of TM6 in a manner analogous to the two arms supporting a gymnast on the rings.

In "still-rings" model, we hypothesized that the positively charged Zn^{2+} interacted with the negatively charged residue D330, thereby disrupting the R302-D330 interaction. Meanwhile, the negatively charged sulfate group of LCAS interacted with the positively charged R303, disrupting the R303-E116 interaction. It was also possible that the sulfate group of LCAS simultaneously engaged both R302 and R303, thereby inducing conformational changes in TM6.

Activation of GPR39 by LCAS induces ERK phosphorylation in primary acinar cells and hepatocytes

Previous results have shown that GPR39 mediates BA-induced Ca^{2+} elevation in acinar cells and plays an important role in BA-induced acute biliary pancreatitis, and the inflammation of acute pancreatitis was significantly reduced in *Gpr39* knockout mice (16). To investigate whether BA induced ERK phosphorylation *via* this receptor, we performed Western analyses on primary acinar cells and hepatocytes from WT and *Gpr39* knockout mice. LCAS treatment significantly increased phosphorylation at the T202/Y204 of ERK1 and T185/Y187 of ERK2 in WT acinar cells ($p < 0.01$, Fig. 7, *A* and *B*). Of note, this upregulation of pERK/total ERK ratios was abolished in *Gpr39* knockout mice (Fig. 7*C*). Given that GPR39 was also highly expressed in hepatocytes (40), we examined this pathway in hepatocytes. Consistent with acinar cells, LCAS significantly increased pERK/total ERK ratios in primary hepatocytes from WT mice (Fig. 7, *D* and *E*). In contrast, this upregulation of pERK/total ERK ratios in *Gpr39* knockout mice was abolished (Fig. 7, *D* and *F*). These results indicate that GPR39 mediated BA signaling to the ERK pathway in pancreatic acinar cells and hepatocytes.

Discussion

We have extended our previous conclusion of GPR39 activation by BAs with electrophysiologic recording in the *Xenopus* oocytes system, investigated Gα proteins recruited by GPR39 after BAs and Zn^{2+} activation, and dissected residues required for GPR39 activation by BA and Zn^{2+}, and ERK signaling by BA-GPR39. These results advance our understanding of molecular signaling mechanisms underlying GPR39 and BAs interactions.

Efforts have been made to find endogenous ligands, exogenous agonists and antagonists of GPR39 (15, 41), Zn^{2+} (13), eicosanoids (42), BAs (16), and the GPNMB protein (43) have been reported as endogenous ligands of GPR39, though some were based on a single assay and some remain controversial. We have succeeded in employing multiple assays from electrophysiologic recording in *Xenopus* oocytes, Ca^{2+} imaging (FLIPR), NanoBiT and ONE-GO, all of which provided results supporting the idea of GPR39 activation by BAs. Taken together, our previous and present results provide the strongest support that BAs activate GPR39.

In mammalian cultured cells, GPR39 exhibits constitutive activity in the absence of exogenous applied ligands (44), and could form heteroreceptor complexes with other GPCRs (45). *Xenopus* oocytes provide a system in which GPR39 showed no constitutive activity. Results from *Xenopus* oocytes supported that LCAS activated GPR39 in a dose-dependent manner. This indicates that GPR39 alone in the cell membrane is sufficient to mediate cellular responses to LCAS. In *Xenopus* oocytes, the EC_{50} for GPR39 activation by Zn^{2+} and LCAS were much higher than those in HEK293T cells using other

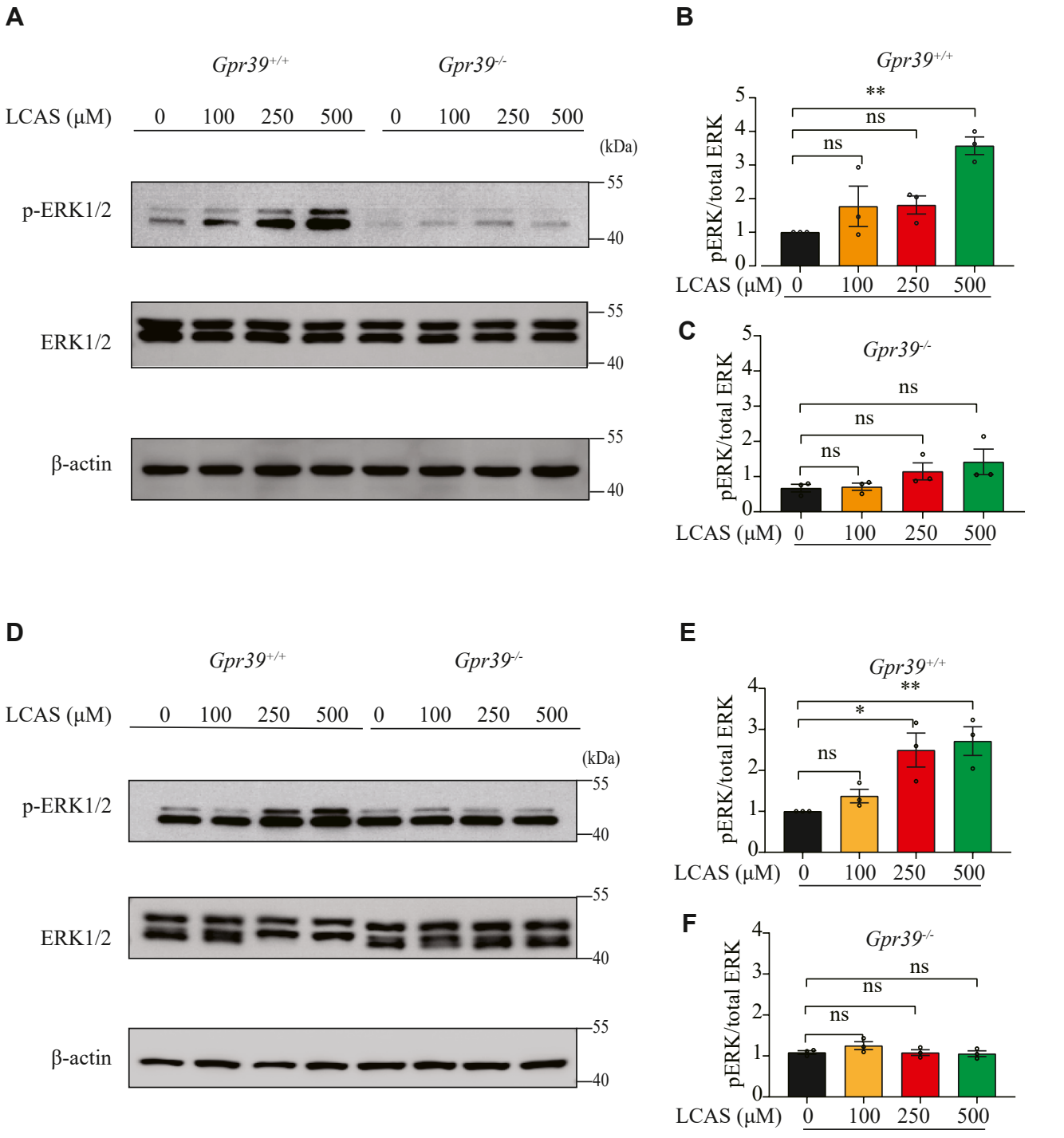

Figure 7. LCAS-induced phosphorylation of ERK1/2 *via* GPR39 in primary pancreatic acinar cells and hepatocytes. *A*, primary pancreatic acinar cells were exposed to the indicated concentrations of LCAS for 1 h. Cell lysates were immunoblotted with antibodies against phospho-ERK1/2 and total ERK. *B* and *C*, band intensities of WT and *Gpr39*$^{-/-}$ mice were quantified in ImageJ, and phospho-ERK/total-ERK ratios were plotted. N = 3, mean ± SD. One-way ANOVA with Tukey's multiple comparisons posttest was made to the untreated group, ** indicates $p < 0.01$, ns indicates $p > 0.05$. The p values of 100 μM LCAS, 250 μM LCAS and 500 μM LCAS *versus* control group in WT mice were 0.3417, 0.3088 and 0.0023. The p values of 100 μM LCAS, 250 μM LCAS and 500 μM LCAS *versus* control group in *Gpr39*$^{-/-}$ mice were 0.9986, 0.3794 and 0.1190. *D*, primary hepatocytes were exposed to the indicated concentrations of LCAS for 10 min. Cell lysates were immunoblotted with antibodies against phospho-ERK1/2 and total ERK. *E* and *F*, band intensities of WT and *Gpr39*$^{-/-}$ mice were quantified in ImageJ, and phospho-ERK/total-ERK ratios were plotted in the *right panel*. N = 3, mean ± SD. One-way ANOVA with Tukey's multiple comparisons posttest was made to the untreated group, ** indicates $p < 0.01$, ns indicates $p > 0.05$. The p values of 100 μM LCAS, 250 μM LCAS and 500 μM LCAS *versus* control group in WT mice were 0.6873, 0.0146 and 0.0069. The p values of 100 μM LCAS, 250 μM LCAS and 500 μM LCAS *versus* control group in *Gpr39*$^{-/-}$ mice were 0.3151, > 0.9999 and 0.9779.

assays. The differences may be attributed to variations in the phospholipid composition of their plasma membranes, affecting receptor conformational changes (46).

GPR39 and GPBAR1 are both expressed in the gastrointestinal tract (6, 47, 48), suggesting potential crosstalk or functional interplay between these two BA-sensing receptors.

GPBAR1, a well-established $G\alpha_s$-coupled receptor, mediates BA-dependent regulation of metabolic processes through cAMP (49–51). We have previously shown that 3-O-sulfation of BAs significantly reduces their ability to activate GPBAR1, thereby attenuating its downstream signaling (16). Here, we report that 3-O-sulfated lithocholic acids (LCAS, TLCAS and GLCAS) can activate $G\alpha_i$ signaling *via* GPR39. Given that $G\alpha_i$ activation suppresses $G\alpha_s$-mediated cAMP production, this raises the possibility that GPR39 may serve as a functional antagonist to GPBAR1 signaling in cells co-expressing them. Thus, BA sulfation not only limits GPBAR1 activation directly but also indirectly modulates its signaling output *via* GPR39-$G\alpha_i$ signaling. This dual regulation may contribute to the spatial and functional specificities of BA signaling within the gastrointestinal tract.

Because of GPR39 expression in tissues such as the liver, the pancreas, and the gastrointestinal tract (9), BA signaling through GPR39 may regulate metabolic and digestive processes. In the gastrointestinal tract, GPR39 activation regulates epithelial tight junctions and pH homeostasis, which are essential for maintaining gut barrier integrity (52). In the liver, GPR39 has been reported to regulate insulin signaling, attenuate liver fibrosis, and reduce inflammatory responses (40). Because BAs are abundantly present in both the intestine and liver (53), whether BA-GPR39 signaling contributes to these functions under physiological or pathological conditions represents an interesting topic for future studies.

The observation that LCAS induced ERK1/2 phosphorylation in primary acinar cells and hepatocytes was abolished in *Gpr39* knockout mice provides a mechanistic entry point to dissect how endogenous BAs, *via* GPR39, modulate functions of cells and organs in the digestive system under physiological and pathological conditions.

Overall, our study provides a comprehensive analysis of signaling pathways activated by BAs through GPR39. Our findings have furthered the understanding of GPR39 and BAs and highlighted the potential for studying BA-GPR39 signaling in physiological and pathological processes.

Experimental procedures

Materials

Chemicals and reagents were purchased from Promega, Sigma-Aldrich or Thermo Fisher unless otherwise specified. Most BAs were from IsoScience. LCAS was obtained from Santa Cruz Biotechnology, while TLCAS and TCAS were acquired from Cayman Chemical. HEK293T cells were maintained in our laboratory under standard conditions.

Animals

Xenopus laevis were purchased from the Research Center for Eco-Environmental Sciences of the Chinese Academy of Sciences and housed in large glass tanks maintained at 18 °C, with no more than five animals per tank. G*pr39* knockout mice were self-propagated in our laboratory (16). All animal procedures were conducted in compliance with the ethical guidelines set forth by the Ethics Committee for Animal Experiments of Peking University.

DNA constructs and site-directed mutagenesis

Mouse GPR39 cDNA was cloned into the pCMV6-Entry vector (OriGene), with an in-frame fusion to mCherry *via* a P2A linker. Site-directed mutagenesis was performed using PCR-based methods, and all mutations were confirmed by Sanger sequencing. For membrane expression of mutants, a 3× HA tag at the N-terminus was added. A large fragment of luciferase was fused to the C-terminus of GPR39 for the NanoBiT assay, and mini-Gα proteins were used as previously described (17). For *Xenopus* oocyte experiments, the pCMV6 vector was replaced by the pCS2 vector, which lacked mCherry and the P2A linker.

Cell culture and transfection

HEK293T cells were cultured in Dulbecco's Modified Eagle Medium (DMEM), supplemented with 1% penicillin-streptomycin (Gibco) and 10% fetal bovine serum (FBS, Vazyme). Cells were maintained in a humidified incubator at 37 °C with 5% CO_2. For transfections, cells were seeded into 96-well plates and transfected with 100 ng of DNA per well using the Lipofectamine 3000 reagent according to the manufacturer's instruction. The DNA-Lipofectamine mixture was incubated for 15 min at room temperature before application to the cells.

NanoBiT assay

The NanoBiT assay was carried out according to a previous report (17). HEK293T cells were co-transfected with 50 ng of the GPR39-large bit plasmid and 50 ng of the mini Gα protein-small bit plasmid. The sequences of β-arrestin1 and β-arrestin2 were reported previously (33). After 24 h of incubation, cells were washed with Hank's Balanced Salt Solution (HBSS) and incubated with 50 μl of HBSS per well containing 1 μM Furimazine (GLPBIO, PBI3939) for 3 min. Baseline measurements were recorded over 10 readings, followed by stimulation with 50 μl BAs (containing 1 μM Furimazine). Luminescence was recorded for 20 subsequent readings at 25 °C using an EnSight Multimode Plate Reader (PerkinElmer). Baselines were determined using the first three measurements, and maximum responses were calculated as the difference between the peak post-stimulation value and the baseline.

ONE-GO assay

The ONE-GO assay was carried out according to a previous report (18). HEK293T cells were transfected with 50 ng of the GPR39 plasmid and 50 ng of the corresponding Gα protein plasmid. After 24 h, cells were washed with HBSS and incubated with 80 μl of HBSS per well containing the Nano-Glo substrate (Promega, cat# N1120, diluted 1:200) for 2 min. Luminescence was measured at 460 ± 40 nm and 535 ± 15 nm using a BioTek Cytation5 plate reader (BioTek Instruments, Inc.) at 28 °C. Cells were subsequently stimulated with 20 μl

of BAs. BRET signals were calculated as the ratio of emission intensities at 535 nm and 460 nm, with baseline values determined from the first three measurements. For kinetic BRET measurements, luminescence was recorded every 0.24 s throughout the experiment, and ΔBRET was calculated by subtracting the pre-stimulation baseline from all subsequent data points.

FLIPR Ca^{2+} imaging assay

Ca^{2+} imaging has been described previously (16). HEK293T cells were seeded in PDL-coated 96-well plates and transfected with cDNAs encoding mutant proteins. After 18 h, cells were washed with HBSS and incubated with 50 μl of HBSS per well containing 2 μg/ml Fluo-8 AM (AAT Bioquest) for 30 min at room temperature. The dye was replaced with an equal volume of HBSS for 5 min before recording. Ca^{2+} responses were imaged using the FLIPR system at room temperature. The recording interval was set to 1 s, and 50 μl of stimulating solution was dispensed at the 30-s mark, followed by 150 s of recording. Baseline values were calculated as the average of the first 20 s, and the responses were determined as the maximum signal minus the baseline.

Xenopus *oocyte electrophysiology*

pCS2-GPR39 plasmid was linearized using the NotI-HF enzyme and purified using the ZYMO DNA clean kit. *In vitro* transcription was performed using the mMESSAGE mMACHINE SP6 Transcription Kit. Oocytes were isolated from *X. laevis* and digested with 2 mg/ml collagenase for 45 min to remove the vitelline membranes. Healthy stage V/VI oocytes were selected for injection and incubated at 18 °C overnight. Injections of 50 nl of mRNA (10 ng per oocyte) were performed using a Nanoject II injector. After 24 h of incubation, electrophysiological recordings were performed using a two-electrode voltage-clamp setup. Oocytes were clamped at −80 mV once the baseline current stabilized. Ligand applications were administered by perfusion using a VC3:4 and 8 Channel Gravity Perfusion System (ALA Scientific) at fixed time intervals. Oocytes were incubated with 100 ng/ml of PTX overnight prior to recording. Both 10 μM YM254890 and 100 μM Caccinh-A01 were pretreated 30 s prior to ligand application.

Primary cell isolation

Acinar cells were prepared according to previous reports (16, 54, 55). HEPES-buffered DMEM (Macklin, D6512) with SBTI (0.1 mg/ml) bubbled with O_2 was used as the dissection buffer. The freshly dissected pancreas was digested with collagenase IV (2 mg/ml) dissolved in the dissection buffer containing BSA (2.5 mg/ml). The pancreas was inflated with the digestion solution, cut into small pieces, and transferred to a flask, which was incubated at 37 °C with shaking at 120 rpm for 10 min. The digestion solution was replaced with 5 ml of fresh solution, and the pancreas was digested for another 30 min, before filtration through a 50 μm nylon mesh into 50 ml centrifuge tubes. Primary hepatocytes were prepared according to previous reports (56). After exposing the inferior vena cava and portal vein, a syringe was inserted into the inferior vena cava, the portal vein was clipped after 2 to 3 s, and the liver was flushed with HBSS until the liver turned white. The perfusion was then switched to a digestive solution with 1 mg/ml liberase. After the liver became soft, a cell scraper was used to collect the hepatocytes. Cells were filtered through a 70 μm cell strainer, centrifuged at 50×*g*, resuspended in 10% Percoll in DMEM before centrifugation at 200×*g*, followed by centrifugation and resuspension. Cells were counted at 3×10^5 cells per well for 6-well plates and 6×10^5 cells for 12-well plates for hepatocytes. After 3 h, the medium was changed and after 16 to 20 h drug treatment could be administered. For Western blot analysis, different concentrations of LCAS were added to cells and proteins were extracted after incubation for the indicated times.

Bioinformatics and protein structure modeling

GPR39 protein sequences of the various species were obtained from NCBI database according to our previous study (16). Multiple sequence alignments were created using *ClustalW* software and the visualization was generated by *Jalview*. Amino acid residue conservation scores were calculated by *Jalview* (57). GPR39 structure modeling was generated by *AlphaFold 3 server* (https://alphafoldserver.com/). The structure modeling was based on the mouse GPR39 protein sequence, with the flexible N- and C- terminal regions omitted. Additionally, the long and flexible ECL2 region was replaced with a shorter segment from the zebrafish GPR39 protein. *Diffdock-L* (https://neurosnap.ai/) was used to perform LCAS docking on GPR39 structure generated by the *AlphaFold 3 server* (38) and the structure was visualized using *PyMol version 3.2*.

Statistical analysis

Statistical analyses were performed with GraphPad Prism 8. All data were expressed as mean ± SD. Comparisons between groups were performed using a two-tailed *t* test, one-way ANOVA or two-way ANOVA. Dose-response curves were fitted to a log (agonist) vs. response four-parameter model using GraphPad Prism 8. A significance threshold of $p < 0.05$ was considered statistically significant.

Data availability

The data supporting the findings of this study are available within the article.

Supporting information—This article contains supporting information includes 5 figures and 2 tables.

Acknowledgments—We are grateful to Dr Yi Xian for the ONE-GO biosensors plasmids, the School of Life Sciences of Peking University for *Xeonpus levies* breeding and the National Center for Protein Science at Peking University for access to instrumentation. Work in the Rao laboratory has never been contaminated by the Chinese Brain Initiative.

Author contributions—Y. R. and Y.H. conceptualization; Y. R., Z. Z., and Y. H formal analysis; Y. H., Z. Z., and C. X investigation; Y. H., Z. Z., and C. X. methodology; Y. H., Z. Z., and C. X. validation; Y. H., Z. Z., and C. X. visualization; Y. H. writing–original draft; Y. R., Z. Z., C. X., and Y. H. writing–review and editing; Y. R. supervision; Y. R. funding acquisition.

Conflict of interest—The authors declare that they have no conflicts of interest with the contents of this article.

Abbreviations—The abbreviations used are: A, alanine; AA, amino acid; BAs, bile acids; Ca^{2+}, calcium; cAMP, cyclic adenosine monophosphate; CaCCs, calcium-activated chloride channels; CNS, central nervous system; EC_{50}, half-maximum concentrations; E_{max}, maximum effect; GFP, green fluorescent protein; GHSR, growth hormone secretagogue receptor; GIRKs, G protein-gated inwardly rectifying potassium channels; GLCAS, glycolithocholic acid 3-sulfate; GPCRs, G protein-coupled receptors; HEK, human embryonic kidney; LCAS, lithocholic acid 3-sulfate; Nluc, nanoluc; TEVC, two-electrode voltage-clamp; TLCAS, taurolithocholic acid 3-sulfate; TM, transmembrane domains; YFP, yellow fluorescent protein; Zn^{2+}, zinc ions.

References

1. Liu, S., Anderson, P. J., Rajagopal, S., Lefkowitz, R. J., and Rockman, H. A. (2024) G protein-coupled receptors: a century of research and discovery. *Circ. Res.* **135**, 174–197
2. Lorente, J. S., Sokolov, A. V., Ferguson, G., Schiöth, H. B., Hauser, A. S., and Gloriam, D. E. (2025) GPCR drug discovery: new agents, targets and indications. *Nat. Rev. Drug Discov.* **24**, 458–479
3. McKee, K. K., Tan, C. P., Palyha, O. C., Liu, J., Feighner, S. D., Hreniuk, D. L., *et al.* (1997) Cloning and characterization of two human G protein-coupled receptor genes (GPR38 and GPR39) related to the growth hormone secretagogue and neurotensin receptors. *Genomics* **46**, 426–434
4. Zhang, M., Chen, T., Lu, X., Lan, X., Chen, Z., and Lu, S. (2024) G protein-coupled receptors (GPCRs): advances in structures, mechanisms, and drug discovery. *Signal. Transduct. Targeted Ther.* **9**, 88
5. Jackson, V. R., Nothacker, H. P., and Civelli, O. (2006) GPR39 receptor expression in the mouse brain. *Neuroreport* **17**, 813–816
6. Moechars, D., Depoortere, I., Moreaux, B., de Smet, B., Goris, I., Hoskens, L., *et al.* (2006) Altered gastrointestinal and metabolic function in the GPR39-obestatin receptor-knockout mouse. *Gastroenterology* **131**, 1131–1141
7. Cohen, L., Sekler, I., and Hershfinkel, M. (2014) The zinc sensing receptor, ZnR/GPR39, controls proliferation and differentiation of colonocytes and thereby tight junction formation in the colon. *Cell Death Dis.* **5**, e1307
8. Dittmer, S., Sahin, M., Pantlen, A., Saxena, A., Toutzaris, D., Pina, A. L., *et al.* (2008) The constitutively active orphan G-protein-coupled receptor GPR39 protects from cell death by increasing secretion of pigment epithelium-derived growth factor. *J. Biol. Chem.* **283**, 7074–7081
9. Dong, X., Tang, S., Zhang, W., Gao, W., and Chen, Y. (2016) GPR39 activates proliferation and differentiation of porcine intramuscular preadipocytes through targeting the PI3K/AKT cell signaling pathway. *J. Recept. Signal. Transduct. Res.* **36**, 130–138
10. Ganay, T., Asraf, H., Aizenman, E., Bogdanovic, M., Sekler, I., and Hershfinkel, M. (2015) Regulation of neuronal pH by the metabotropic Zn(2+)-sensing Gq-coupled receptor, mZnR/GPR39. *J. Neurochem.* **135**, 897–907
11. Sunuwar, L., Asraf, H., Donowitz, M., Sekler, I., and Hershfinkel, M. (2017) The Zn(2+)-sensing receptor, ZnR/GPR39, upregulates colonocytic Cl(-) absorption, via basolateral KCC1, and reduces fluid loss. *Biochim. Biophys. Acta Mol. Basis Dis.* **1863**, 947–960
12. Yang, P., Feng, Q., Meng, L., Tang, R., Jiang, Y., Liu, H., *et al.* (2022) The mechanism underlying the TC-G 1008 rescue of reactive oxygen species (ROS)-induced osteoblast apoptosis by the upregulation of peroxiredoxin 1. *Int. J. Biochem. Cell Biol.* **151**, 106276
13. Holst, B., Egerod, K. L., Schild, E., Vickers, S. P., Cheetham, S., Gerlach, L. O., *et al.* (2007) GPR39 signaling is stimulated by zinc ions but not by obestatin. *Endocrinology* **148**, 13–20
14. Yasuda, S., Miyazaki, T., Munechika, K., Yamashita, M., Ikeda, Y., and Kamizono, A. (2007) Isolation of Zn2+ as an endogenous agonist of GPR39 from fetal bovine serum. *J. Recept. Signal. Transduct. Res.* **27**, 235–246
15. Doboszewska, U., Maret, W., and Wlaź, P. (2024) GPR39: an orphan receptor begging for ligands. *Drug Discov. Today* **29**, 103861
16. Zi, Z., and Rao, Y. (2024) Discoveries of GPR39 as an evolutionarily conserved receptor for bile acids and of its involvement in biliary acute pancreatitis. *Sci. Adv.* **10**, eadj0146
17. Laschet, C., Dupuis, N., and Hanson, J. (2019) A dynamic and screening-compatible nanoluciferase-based complementation assay enables profiling of individual GPCR-G protein interactions. *J. Biol. Chem.* **294**, 4079–4090
18. Janicot, R., Maziarz, M., Park, J. C., Zhao, J., Luebbers, A., Green, E., *et al.* (2024) Direct interrogation of context-dependent GPCR activity with a universal biosensor platform. *Cell* **187**, 1527–1546.e5
19. Hansen, K. B., and Bräuner-Osborne, H. (2009) Xenopus oocyte electrophysiology in GPCR drug discovery. *Methods Mol. Biol.* **552**, 343–357
20. Ivorra, I., Alberola-Die, A., Cobo, R., González-Ros, J. M., and Morales, A. (2022) Xenopus oocytes as a powerful cellular model to study foreign fully-processed membrane proteins. *Membranes* **12**, 986
21. O'Connor, E. C., Kambara, K., and Bertrand, D. (2024) Advancements in the use of xenopus oocytes for modelling neurological disease for novel drug discovery. *Expert Opin. Drug Discov.* **19**, 173–187
22. Taniguchi, M., Nagai, K., Arao, N., Kawasaki, T., Saito, T., Moritani, Y., *et al.* (2003) YM-254890, a novel platelet aggregation inhibitor produced by Chromobacterium sp. QS3666. *J. Antibiot.* **56**, 358–363
23. De La Fuente, R., Namkung, W., Mills, A., and Verkman, A. S. (2008) Small-molecule screen identifies inhibitors of a human intestinal calcium-activated chloride channel. *Mol. Pharmacol.* **73**, 758–768
24. Flock, T., Hauser, A. S., Lund, N., Gloriam, D. E., Balaji, S., and Babu, M. M. (2017) Selectivity determinants of GPCR-G-protein binding. *Nature* **545**, 317–322
25. Seyedabadi, M., Ghahremani, M. H., and Albert, P. R. (2019) Biased signaling of G protein coupled receptors (GPCRs): molecular determinants of GPCR/transducer selectivity and therapeutic potential. *Pharmacol. Ther.* **200**, 148–178
26. Liu, J., Tang, H., Xu, C., Zhou, S., Zhu, X., Li, Y., *et al.* (2022) Biased signaling due to oligomerization of the G protein-coupled platelet-activating factor receptor. *Nat. Commun.* **13**, 6365
27. Shao, Z., Shen, Q., Yao, B., Mao, C., Chen, L. N., Zhang, H., *et al.* (2022) Identification and mechanism of G protein-biased ligands for chemokine receptor CCR1. *Nat. Chem. Biol.* **18**, 264–271
28. Hauser, A. S., Avet, C., Normand, C., Mancini, A., Inoue, A., Bouvier, M., *et al.* (2022) Common coupling map advances GPCR-G protein selectivity. *eLife* **11**, e74107
29. Syrovatkina, V., Alegre, K. O., Dey, R., and Huang, X. Y. (2016) Regulation, signaling, and physiological functions of G-proteins. *J. Mol. Biol.* **428**, 3850–3868
30. Inoue, A., Raimondi, F., Kadji, F. M. N., Singh, G., Kishi, T., Uwamizu, A., *et al.* (2019) Illuminating G-Protein-Coupling selectivity of GPCRs. *Cell* **177**, 1933–1947.e25
31. Rajagopal, S., and Shenoy, S. K. (2018) GPCR desensitization: acute and prolonged phases. *Cell. Signal.* **41**, 9–16
32. Kahsai, A. W., Shah, K. S., Shim, P. J., Lee, M. A., Shreiber, B. N., Schwalb, A. M., *et al.* (2023) Signal transduction at GPCRs: allosteric activation of the ERK MAPK by β-arrestin. *Proc. Natl. Acad. Sci. U. S. A.* **120**, e2303794120
33. Zhao, C., Wang, H., Liu, Y., Cheng, L., Wang, B., Tian, X., *et al.* (2023) Biased allosteric activation of ketone body receptor HCAR2 suppresses inflammation. *Mol. Cell* **83**, 3171–3187.e7

34. Mohanty, I., Mannochio-Russo, H., Schweer, J. V., El Abiead, Y., Bittremieux, W., Xing, S., *et al.* (2024) The underappreciated diversity of bile acid modifications. *Cell* **187**, 1801–1818.e20
35. Perino, A., and Schoonjans, K. (2022) Metabolic messengers: bile acids. *Nat. Metab.* **4**, 416–423
36. Wahlström, A., Sayin, S. I., Marschall, H. U., and Bäckhed, F. (2016) Intestinal crosstalk between bile acids and microbiota and its impact on host metabolism. *Cell Metab.* **24**, 41–50
37. Zhou, Q., Yang, D., Wu, M., Guo, Y., Guo, W., Zhong, L., *et al.* (2019) Common activation mechanism of class A GPCRs. *eLife* **8**, e50279
38. Corso, G., Deng, A., Fry, B., Polizzi, N., Barzilay, R., and Jaakkola, T. (2024) Deep confident steps to new pockets: strategies for docking generalization. *ArXiv*. https://doi.org/10.48550/arXiv.2402.18396
39. Frimurer, T. M., Mende, F., Graae, A. S., Engelstoft, M. S., Egerod, K. L., Nygaard, R., *et al.* (2017) Model-based discovery of synthetic agonists for the Zn2+-sensing G-protein-coupled receptor 39 (GPR39) reveals novel biological functions. *J. Med. Chem.* **60**, 886–898
40. Shendge, A. K., Sekler, I., and Hershfinkel, M. (2024) ZnR/GPR39 regulates hepatic insulin signaling, tunes liver bioenergetics and ROS production, and mitigates liver fibrosis and injury. *Redox Biol.* **78**, 103403
41. Cheng, Y., Zhao, C., Bin, Y., Liu, Y., Cheng, L., Xia, F., *et al.* (2024) The pathophysiological functions and therapeutic potential of GPR39: focus on agonists and antagonists. *Int. Immunopharmacol* **143**, 113491
42. Alkayed, N. J., Cao, Z., Qian, Z. Y., Nagarajan, S., Liu, X., Nelson, J. W., *et al.* (2022) Control of coronary vascular resistance by eicosanoids via a novel GPCR. *Am. J. Physiol. Cell Physiol.* **322**, C1011–C1021
43. Ramadoss, S., Qin, J., Tao, B., Thomas, N. E., Cao, E., Wu, R., *et al.* (2024) Bone-marrow macrophage-derived GPNMB protein binds to orphan receptor GPR39 and plays a critical role in cardiac repair. *Nat. Cardiovasc. Res.* **3**, 1356–1373
44. Holst, B., Holliday, N. D., Bach, A., Elling, C. E., Cox, H. M., and Schwartz, T. W. (2004) Common structural basis for constitutive activity of the ghrelin receptor family. *J. Biol. Chem.* **279**, 53806–53817
45. Tena-Campos, M., Ramon, E., Borroto-Escuela, D. O., Fuxe, K., and Garriga, P. (2015) The zinc binding receptor GPR39 interacts with 5-HT1A and GalR1 to form dynamic heteroreceptor complexes with signaling diversity. *Biochim. Biophys. Acta* **1852**, 2585–2592
46. Hou, X., Zhang, D. D., Yuvaraj, J. K., Corcoran, J. A., Andersson, M. N., and Löfstedt, C. (2020) Functional characterization of odorant receptors from the moth Eriocrania semipurpurella: a comparison of results in the Xenopus oocyte and HEK cell systems. *Insect Biochem. Mol. Biol.* **117**, 103289
47. Alemi, F., Poole, D. P., Chiu, J., Schoonjans, K., Cattaruzza, F., Grider, J. R., *et al.* (2013) The receptor TGR5 mediates the prokinetic actions of intestinal bile acids and is required for normal defecation in mice. *Gastroenterology* **144**, 145–154
48. Poole, D. P., Godfrey, C., Cattaruzza, F., Cottrell, G. S., Kirkland, J. G., Pelayo, J. C., *et al.* (2010) Expression and function of the bile acid receptor GpBAR1 (TGR5) in the murine enteric nervous system. *Neurogastroenterol. Motil.* **22**, e227–e818
49. Kawamata, Y., Fujii, R., Hosoya, M., Harada, M., Yoshida, H., Miwa, M., *et al.* (2003) A G protein-coupled receptor responsive to bile acids. *J. Biol. Chem.* **278**, 9435–9440
50. Chiang, J. Y. L., and Ferrell, J. M. (2019) Bile acids as metabolic regulators and nutrient sensors. *Annu. Rev. Nutr.* **39**, 175–200
51. Perino, A., Demagny, H., Velazquez-Villegas, L., and Schoonjans, K. (2021) Molecular physiology of bile acid signaling in health, disease, and aging. *Physiol. Rev.* **101**, 683–731
52. Pongkorpsakol, P., Buasakdi, C., Chantivas, T., Chatsudthipong, V., and Muanprasat, C. (2019) An agonist of a zinc-sensing receptor GPR39 enhances tight junction assembly in intestinal epithelial cells via an AMPK-dependent mechanism. *Eur. J. Pharmacol.* **842**, 306–313
53. Ahmad, T. R., and Haeusler, R. A. (2019) Bile acids in glucose metabolism and insulin signalling - mechanisms and research needs. *Nat. Rev. Endocrinol.* **15**, 701–712
54. Orabi, A. I., Muili, K. A., Wang, D., Jin, S., Perides, G., and Husain, S. Z. (2013) Preparation of pancreatic acinar cells for the purpose of calcium imaging, cell injury measurements, and adenoviral infection. *J. Vis. Expt* **77**, e50391
55. Gout, J., Pommier, R. M., Vincent, D. F., Kaniewski, B., Martel, S., Valcourt, U., *et al.* (2013) Isolation and culture of mouse primary pancreatic acinar cells. *J. Vis. Expt* **78**, e50514
56. Charni-Natan, M., and Goldstein, I. (2020) Protocol for primary mouse hepatocyte isolation. *STAR Prots* **1**, 100086
57. Waterhouse, A. M., Procter, J. B., Martin, D. M., Clamp, M., and Barton, G. J. (2009) Jalview Version 2–a multiple sequence alignment editor and analysis workbench. *Bioinformatics* **25**, 1189–1191